ADVANCED ENGINEERING MATERIALS
www.aem-journal.com

4D Printing of PLA/PBS Biopolymers: Impact of Polymer Grade Variations on Thermomechanical Performance

*Ava Ghalayaniesfahani, Betty Oostenbrink, Han van Kasteren, and Mehrshad Mehrpouya**

The adoption of biobased polymers is growing in the additive manufacturing industry, offering alternatives to petrochemical-based plastics, known for their environmental impact. However, finding a single polymer with all desirable properties is challenging. Blending polymers allows for the combination of distinct features, optimizing performance for specific applications. This study formulates two biopolymer blends of poly(butylene succinate) (PBS) and poly(lactic acid) (PLA) (80/20 wt%) using different PBS grades to examine their effects on thermomechanical and functional properties. The addition of PLA, a shape memory polymer, enables dynamic changes in 3D printed structures, causing them to deform under stimuli and revert to their original shape—an effect known as 4D printing. The blend pellets are then used in filament extrusion, and smart sandwich samples are produced using fused filament fabrication. The thermomechanical and functional characteristics of the printed samples are evaluated. This research highlights the differences arising from using different PBS grades in 3D printed structures with high energy absorption. Results show that melt flow rate is a crucial factor, significantly affecting the thermomechanical and shape memory behavior, with variation between 86% and 93%.

1. Introduction

The extensive use of synthetic polymers derived from petrochemical resources has had a detrimental impact on our environment, contributing significantly to ecological solid waste issues.[1] The growing popularity of 3D printing has led to an increased demand for sustainable raw materials. The emergence of biopolymers offers a promising solution to this challenge.[1–3] Bioplastics can be broadly categorized into two types: biobased and biodegradable polymers. Biobased plastics are sourced from renewable bioresources like vegetable oils, microbiota, corn starch, or bacterial fermentation, making them more environmentally friendly. However, biodegradable polymers constitute a distinct category that decomposes into natural byproducts, including biomass, inorganic salt, gases, water, and inorganic salts, once their specific purpose has been fulfilled.[4,5] These bioplastics are increasingly recognized as potential replacements for synthetic counterparts, offering solutions to environmental challenges. They are gaining significant attention for their diverse applications in the development of environmentally friendly products.

One of the key indicators of a plastic's processability is its melt flow rate (MFR), which reflects the ease of material flow. This characteristic holds particular significance in the additive manufacturing (AM) industry, where smooth material flow is essential for quality and efficiency.[6,7] While the MFR of a sample is primarily influenced by its average molecular weight (MW), this correlation can be significantly impacted by variables like the molecular weight distribution (MWD) and the extent of long-chain branching. Polymer grades are often distinguished by their melt flow index (MFI) and MFR values. Extrusion grades, suitable for pipe, film, and blow-molding applications often exhibit broad MWDs or high MFRs. This characteristic contributes to favorable mechanical properties and improved processability. Conversely, injection molding grades necessitate a very narrow MWD and lower MFRs to minimize shrinkage during the molding process.

The main objective of this research is to study the effect of polymer grades on the thermomechanical and functional properties of the blend. These blends are composed of 80% poly(lactic acid) (PLA), a widely used biobased polymer. There are at least two key aspects of PLA driving this research interest. First, PLA, as a biobased and biodegradable polymer, can be sourced entirely from natural resources, such as sugarcane, corn, wheat, or rice and also decomposed to natural byproducts.[8] Second, PLA is a shape memory polymer, capable of transitioning from a temporary state to a memorized permanent initial one when stimulated by suitable stimuli.[9] This technology marks a revolutionary shift in the AM industry with the emergence of "4D printing,"

A. Ghalayaniesfahani, M. Mehrpouya
Faculty of Engineering Technology
University of Twente
P.O. Box 217, 7500 AE Enschede, The Netherlands
E-mail: m.mehrpouya@utwente.nl

B. Oostenbrink, H. van Kasteren
Centre of Expertise Materials and Energy Transitions
Avans University of Applied Sciences
Lovensdijkstraat 63, 4818 AJ Breda, The Netherlands

The ORCID identification number(s) for the author(s) of this article can be found under https://doi.org/10.1002/adem.202401705.

DOI: 10.1002/adem.202401705

integrating smart materials capable of shape-shifting transformations over time in response to external stimuli.[9–12] PLA exhibits a remarkable shape memory property along with outstanding mechanical strength, including high strength and modulus.[4,5,13,14] However, its application is constrained by factors such as poor thermal stability, flexibility, and crystallization ability, as well as brittleness, which limit its utility.[15–19] Hence, addressing this issue may involve the inclusion of biobased reinforcements, such as cellulose nanofibers, or the blending of PLA with more ductile and flexible biopolymers as potential solutions; however, it is crucial to ensure that these methods do not alter the biobased nature of the material.

For this reason, poly(butylene succinate) (PBS) biopolymer, categorized under aliphatic polyesters and sourced from natural resources like sugarcane, cassava, and corn, is incorporated into this study. PBS demonstrates compostability at open-air landfill sites under ambient conditions, eliminating the need for specialized composting facilities. PBS stands out as one of the most interesting biopolymers due to its well-balanced combination of flexibility, ductility, toughness, impact, and chemical resistance.[20–23] However, its limited Young's modulus and its vulnerability to sudden degradation at elevated temperatures have rendered it impractical for use as a filament in the fused filament fabrication (FFF) 3D printing industry.[23] Hence, to take advantage of its properties, it should be necessarily blended or reinforced with other polymers, fillers, and additives. This is done to address challenges related to improved processability, increased stiffness, and overall enhanced mechanical strength. While PLA boasts good mechanical properties such as high yield strength, it tends to be brittle. Conversely, PBS exhibits flexibility but comes with a low Young's modulus and susceptibility to thermal degradation at elevated temperatures. These two polymers are compatible and through blending of these two biopolymers, we achieve a sustainable, eco-friendly blend that allows us to mitigate the weaknesses of each side and capitalize on their complementary properties. Our previous study investigated the influence of varying weight ratios of PBS and PLA, along with the presence of compatibilizer, on the thermomechanical properties, shape recovery, and energy absorption of 4D printed biobased shape memory sandwich structures.[24] While other studies have also investigated the influence of varying proportions of these two polymers in PLA/PBS blends and assessed their properties,[25–28] this research introduces novelty by examining the impact of different polymer grades, each equally represented within the blend, on thermomechanical and functional properties of smart 3D printed sandwich structures. These structures are manufactured through a multistep process, including compounding, pelletizing, filament extrusion, and 3D printing.

2. Experimental Section

2.1. Biopolymer Blend

This study compares the thermomechanical and microstructure properties of two distinct blends of PLA/PBS biopolymers. For this purpose, first, two different blends of PLA and PBS biopolymers are prepared by melt-mixing compounding and then pelletized. The composition in the two blends is consistent, comprising 80% PLA and 20% PBS by weight. This ratio is concluded from our previous study,[24] as they showed a better mechanical performance compared to the other blends. Both blends utilize the same grade of PLA pellets, but they incorporate two different grades of PBS pellets (see **Table 1**). The PLA used in this study is Ingeo Biopolymer 4032 D (Reflow, The Netherlands) while the PBS grades employed are BioPBS FZ71PM and BioPBS FZ91PM (Reflow, The Netherlands). The MFR of PBSFZ91 is 5 g/10 min, while in FZ71 it is more than 4 times higher (22 gr/10 min). BioPBS is suitable for processing by coating, blown film extrusion, and injection molding. It finds applications in various fields such as paper coatings, sealants in flexible packaging, hot beverage cups, boxes, and utensils for freshly cooked food.

Table 1. Material properties and grades of PLA, BioPBS FZ91, and BioPBS FZ71.

Properties	Unit	PLA (4032D)	BioPBS FZ91	BioPBS FZ71
Density	$g\,cm^{-1}$	1.24	1.26	1.26
MFR (190 °C, 2.16 kg)	$g\,10^{-1}\,min$	7	5	22
Melting point	°C	162	115	115
Glass transition point	°C	60	−30	−28.5
Yield strength	MPa	60	40	40

2.2. Manufacturing Processes

2.2.1. Compounding Process

The initial phase of manufacturing involves the production of blended pellets through melt-mixing. Before melt compounding, batches of PLA and PBS pellets undergo a drying process at 80 °C for 24 h to mitigate the impact of moisture during processing. Two specific blends with 80 wt% PLA and 20 wt% PBS, namely, PLA/PBS FZ71 and PLA/PBS FZ91, are then crafted through melt compounding. This compounding process takes place on a dual screw extruder (Collin ZK 25, Germany), featuring a 25 mm screw diameter and an L/D ratio of 18. The four internal heaters are precisely set at temperatures of 180–190–190–180 °C while maintaining a screw speed of 40 rpm. Materials are added into the compounder at a rate of 100 g/3 min ($33\,g\,min^{-1}$). The internal pressure of the compounder is consistently controlled and the extrusion parameters were adjusted to keep the internal pressure at 65–70 bar. Subsequently, the extruded material is carefully guided through a water bath (WB 850, Germany) for cooling, and then the blended pellets are pelletized with Pelletizer (CSG 171, Germany) and collected.

2.2.2. Filament Extrusion Process

After the full batch of blended pellets is processed, the collected pellets are dried at 80 °C for 24 h and then used in a filament extruder (3DEVO, model Composer 450, The Netherlands) to produce filaments with a diameter of 1.75 mm. This machine features four heaters internally, positioned from the extruder to the nozzle tip and labeled based on different temperatures

(*T*) between *T*4 and *T*1. Since the majority of the blend is PLA, we used the original extruder process parameters defined for pure PLA to make PLA/PBS filaments. Based on the observed quality of the extruded filament, the parameters have been adjusted, resulting in final heater temperatures set at 180–185–190–180 °C, with a screw speed of 4.9 rpm and fan speed of 70% for all PLA/PBS blended pellets. For pure PLA blends, one of the heater temperatures (*T*4) is set to 170 °C, with a screw speed of 3.5 rpm and fan speed of 70%. **Table 2** represents *T*4 to *T*1 which are the temperatures of the corresponding heating chambers, besides screw and fan speed for each batch of materials extrusion.

2.2.3. 3D Printing Process

In the last step of manufacturing, the samples are 3D printed using pure PLA, PLA/PBS FZ71, and PLA/PBS FZ91 filaments via FFF 3D printer (Creality 10 V3, China). All samples are designed by SolidWorks 2020 (Dassault Systèmes SolidWorks Corporation, USA), and the printing parameters are adjusted in Ultimaker Cura 4.11.0 (Ultimaker B.V., The Netherlands). As the blend consists of 80 wt% PLA, printing is started by the default process parameters for PLA. The only parameter in need of tuning is the printing speed which is set at the lowest one (50 mm s^{-1}) in the recommended range. The 3D printing process parameters are represented in **Table 3**. As all the blends contain 80 wt% PLA, and to ensure a more accurate comparison of properties in the subsequent characterization steps, the thermomechanical processing was kept as uniform as possible across all samples, and the printing parameters are the same both for PLA and PLA/PBS blend samples.

2.3. Material Design Strategy

In this study, the final design entails a 3D printed sandwich structure. The configuration and design of unit cells within sandwich structures are essential factors that affect both mechanical and functional characteristics. These parameters vary depending on the specific application for which they are intended; these unit cells can be customized to meet particular requirements. In this research, a re-entrant structure is selected. Re-entrant auxetic structures are characterized by intricate geometric patterns that yield remarkable mechanical properties. Unlike traditional auxetic structures, which expand in multiple directions when stretched, re-entrant auxetic structures feature internal configurations that lead to enhanced auxetic behavior. This unique design consists of nested or interlocking units, creating a network of interconnected elements that respond to mechanical stimuli in unconventional ways.[29,30] These structures exhibit exceptional properties such as high energy absorption, superior flexibility, and enhanced load distribution. These attributes make them promising candidates for a wide range of applications including protective clothing, impact-resistant materials, and flexible electronics.[29,31,32] **Figure 1** depicts the isometric and front view of re-entrant sandwich structures.

In summary, all manufacturing steps and their related sequence, from polymer blending to filament extrusion and the printing process, are illustrated in **Figure 2**.

Table 2. Filament extruder parameters for PLA and PLA 80/PBS 20 filament production.

Material	*T*4 [°C]	*T*3 [°C]	*T*2 [°C]	*T*1 [°C]	Screw speed [rpm]	Fan speed [%]
PLA	170	185	190	180	3.5	70
PLA/PBS	180	185	190	180	4.9	70

Table 3. Process parameters of FFF 3D printer for printing the samples.

Printing temperature [°C]	Build plate temperature [°C]	Printing speed [mm s^{-1}]	Cooling rate [%]	Layer height [mm]	Infill density [%]
200	60	50	100	0.2	100

2.4. Characterization Process

Following each manufacturing step, it is crucial to assess the quality of the produced component as the characteristics of manufactured material significantly impact the feasibility and quality of subsequent manufacturing steps. In this research, there exist three distinct manufacturing phases: initially compounding blended pellets, followed by filament production, and finally, the 3D printing process. These manufacturing steps are all thermomechanical processes with the potential to impact material properties at each step, highlighting the significance of evaluation and characterization.

2.4.1. Visual Analysis and Scanning Electron Microscopy

The first characterization is to visually analyze the manufactured structure. In this regard, a Digital Microscope (Keyence, VHX-7000N, Belgium) is utilized to capture optical microscopy images of the 3D printed structure, especially at the connection points and the junction of layers to check the printing quality. Additionally, scanning electron microscopy (SEM) (JEOL JSM-7200F, Jeol Ltd., Japan) is used to get a better view of the microscopy morphology. To achieve this, three pieces of each filament from different parts are cut and dried in an oven at 80 for 24 h before the microscopy to eliminate any moisture. To have a smooth fracture surface, they are cryofractured using liquid nitrogen. To this end, all samples were stored in liquid nitrogen for 5 min before breaking. Then the fractured surfaces are coated by a thin layer of gold through sputtering to make the samples conductive for electron microscopy and analyzed with backscattered electron detector and secondary electron detector at magnifications of 5000x.

2.4.2. Thermal Analysis

To determine and compare the thermal properties of the blends and PLA, including the glass transition temperature, crystallization, and melting point of both the blends and pure PLA, a differential scanning calorimeter (DSC) (DSC 250, TA Instruments, USA) is utilized. For each test, small pieces (4–7 mg) of 3D

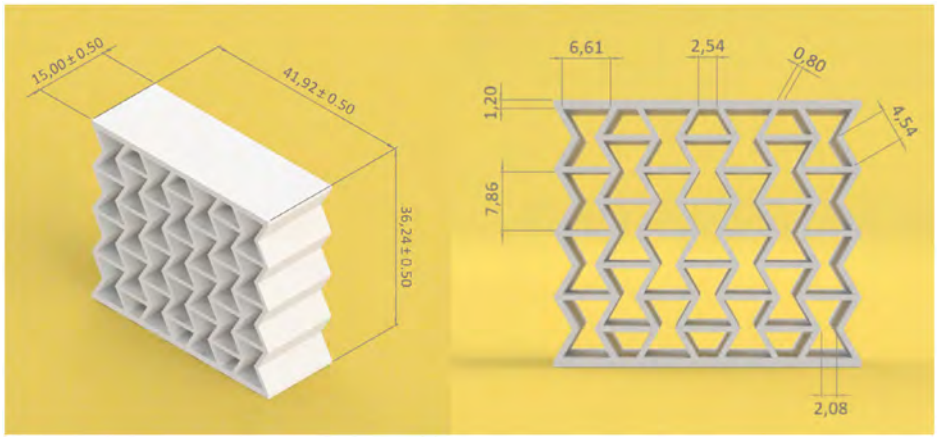

Figure 1. Isometric and front view with dimensions of the re-entrant sandwich structure (all dimensions are in mm).

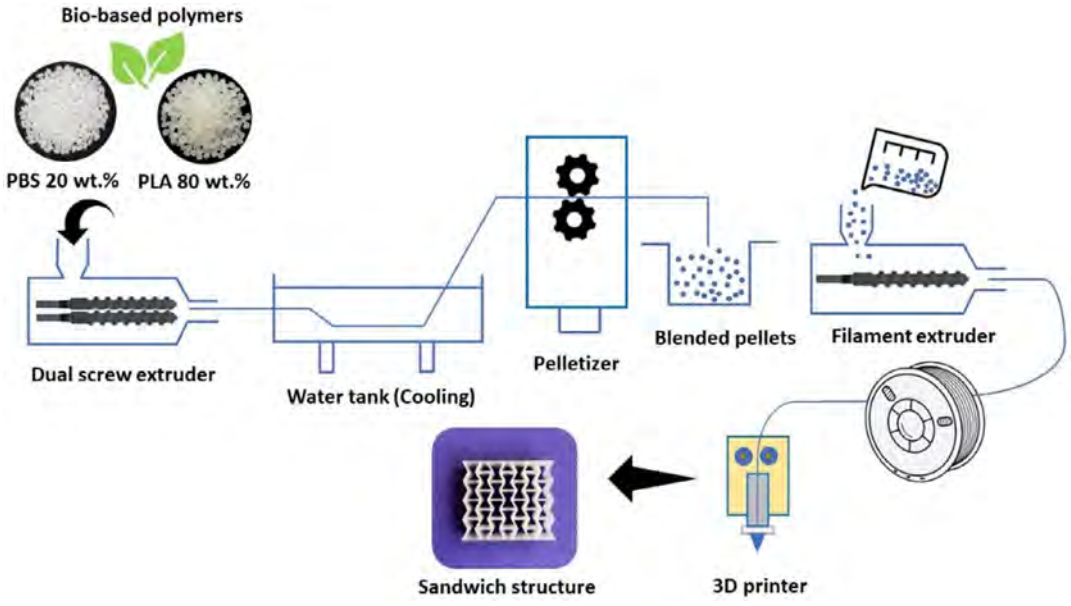

Figure 2. Graphical illustration of manufacturing steps; mixing PLA and PBS pellets, compounding, filament extrusion, and 3D printing sandwich structures.

printed structures are cut and placed in the pans. All test samples undergo heating under a nitrogen atmosphere, ranging from 25 to 200 °C at a heating rate of 10 °C min^{-1}.

2.4.3. Mechanical Analysis

To investigate the quality and mechanical properties of the produced filament, dogbone-shaped samples are 3D printed in accordance with ISO 37:2017 standard, featuring infill lines oriented along their length and in parallel with the tensile direction. This test is done by the Zwicki Line universal testing machine (ZwickRoell, The Netherlands) equipped with a 5 kN load cell. To capture the stress–strain trends, TestXpert3 software (ZwickRoell, The Netherlands) is utilized. These experiments are conducted under standard ambient conditions until the samples are broken.

Compression analysis is also conducted to assess and compare the mechanical properties of three different 3D printed sandwich structures. For compression tests, the same testing facility is employed in order to measure the absorbed and dissipated energy during the cyclic test. During the tests, the deformation speed is set at 4 mm min^{-1}, with an initial preload fixed at 0.5 N. The maximum deformation limit is 50% of the initial length (36.20 mm) which is beyond the densification limit. These experiments are conducted under standard ambient conditions, and each test is repeated 3 times for all samples to ensure the reproducibility and consistency of the results.

2.4.4. Shape Recovery Testing

Since PLA is the primary material in the blends and possesses shape memory properties, the study examines and compares the shape recovery of the samples after programming via cyclic compression tests to assess the shape memory performance of the new biopolymers (see Video 1, Supporting Information). To evaluate the response of the smart sandwich structures to thermal stimuli, all deformed samples were immersed in a temperature-controlled water bath (Julabo, CORIO CD-BT19, Germany) set to 70 °C for 60 s. After heating, the samples are delicately extracted from the water bath and left to recover under ambient conditions. The regained height of the cellular structures is then measured. Subsequently, the data obtained from these experiments are analyzed to collect insights into the materials' shape memory recovery ratios. The shape recovery ratio, often expressed as a percentage, quantifies how well a shape memory material or structure returns to its original shape after undergoing deformation Equation (1):

$$\text{Shape recovery ratio} = \frac{\text{Original dimension} - \text{irrecovered dimension}}{\text{Original dimension}} \times 100 \quad (1)$$

3. Results and Discussion

3.1. Visual Analysis

Figure 3 shows images of the 3D-printed PLA/PBS samples, highlighting strong adhesion between the layers and the structural integrity of the cellular formations. Notably, the images reveal the absence of defects, particularly in the corners and attachment points, confirming the high quality of the printing process. It is important to mention that what might appear as gaps in the horizontal hinges are not actual gaps, but optical artifacts resulting from the transparency of the materials used in 3D printing.

3.2. SEM

Figure 4 presents that all the blends exhibit sea–island structure. There are interfaces between dispersed PBS as circles and PLA matrix, which shows the blend is immiscible. The presence of microvoids is observed in both filaments, possibly attributable to moisture evaporation during extrusion resulting from insufficient drying before analysis. Some small holes might be where the PBS particles got out completely during the cryofracture process which is evidence of interfacial debonding. To compare the size of the dispersed phase based on the viscosity ratio of the blends, it is important to note that the polymer matrix is the same for both blends. Since PBS FZ71 has a higher MFI and lower viscosity than PBS FZ91, the blend with PBS FZ71 will have a higher viscosity ratio. As the viscosity ratio increases, the interfacial tension between PLA and PBS decreases. This reduction in interfacial tension leads to an increase in the size of the dispersed phase in the blend with PBS FZ71.[33–35] Therefore, the blend with PBS FZ71, which has a higher MFI, lower viscosity, and lower MW, exhibits larger PBS domains in the matrix, with an average size of 0.36 μm. This finding is consistent with the previous research, which shows that the size of a more viscous dispersed phase in the same matrix is smaller compared to a less viscous one.[36] For the blend with PBS FZ91, which has a lower MFI and higher viscosity, the dispersed spheres in the matrix are more compact and finer, with an average size of 0.20 μm. These spheres also exhibit a greater tendency to move within the matrix, likely due to the easier breakage of the dispersed phase at similar shear rates compared to the blend with a higher viscosity ratio.

3.3. Thermal Analysis

Figure 5 depicts the results of the DSC test for extruded filaments. The findings indicate that incorporating PBS into the PLA matrix has a direct impact on its thermal characteristics, resulting in a slight decrease in transition temperatures. This change is linked to the creation of an immiscible system and the separate crystallization of the polymers within the blend.

To compare the blends, they show almost the same thermal outcomes as both of them are made from the same amount of two polymers. However, the interesting part is about the shift in heat flow they show. The blend sample with PBS FZ71 indicates a higher value in normalized heat flow at the same temperature compared to the one with PBS FZ91. Since PBS FZ71 has

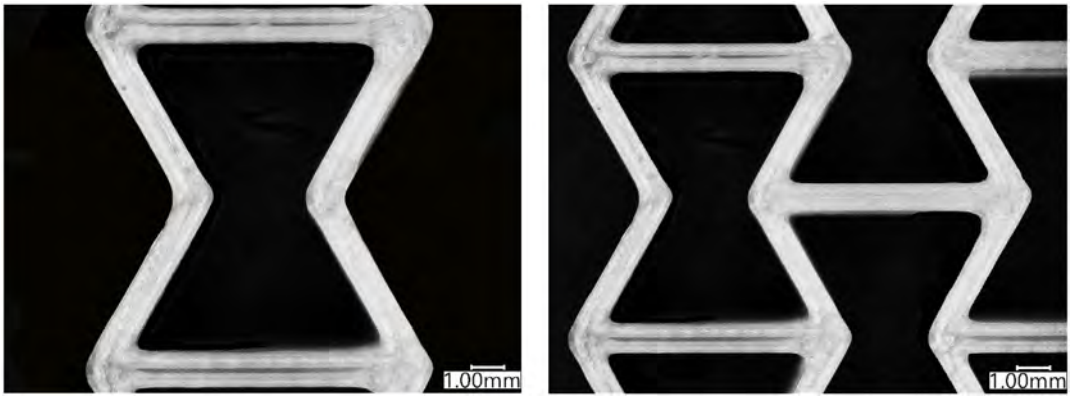

Figure 3. The images of re-entrant PLA/PBS sandwich structures fabricated by FFF 3D printer.

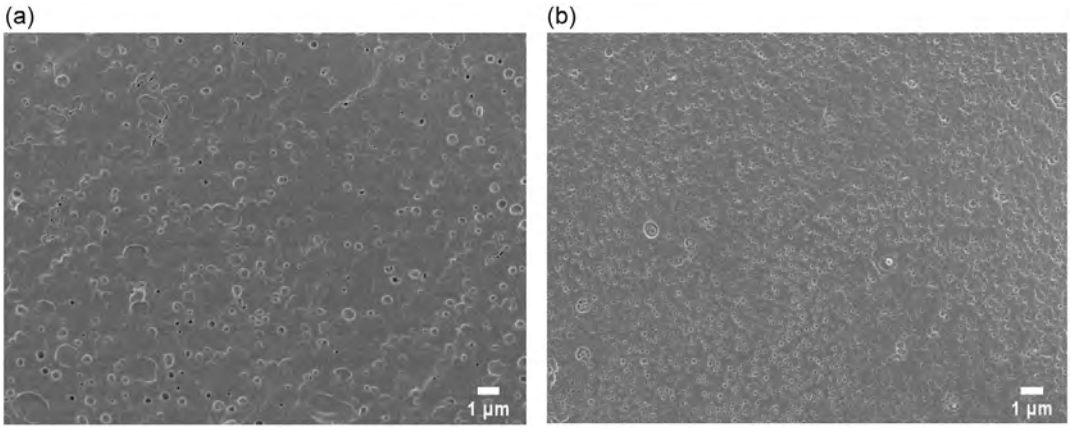

Figure 4. SEM images of a) PLA/PBS FZ71 and b) PLA/PBS F91. Both blends are composed of 80 wt% PLA and 20 wt% PBS.

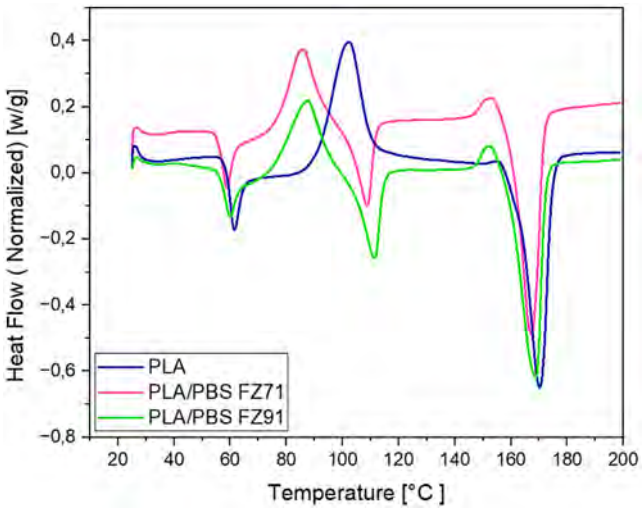

Figure 5. DSC curves of three extruded filaments, comprising PLA, PLA/PBS FZ71, and PLA/PBS FZ91.

lower MW, and the chains are shorter, there is more space between them, which results in easier movements and higher heat flow. However, the enthalpy of crystallization and melting of both blends are quite similar. To better understand this difference, **Table 4** presents the DSC data of the PLA and PLA/PBS blend samples, including precise temperature outputs such as glass transition temperature (T_g), cold crystallization temperature (T_{cc}), and melting temperature (T_m).

3.4. Tensile Test

The mechanical properties of the manufactured sandwich structures are assessed through tensile and compression tests. As shown in **Figure 6**, the results indicate that pure PLA has the highest yield strength, ≈57 MPa, among all the test samples. Between the two PLA/PBS blends, the one containing PBS, designated as FZ91, demonstrates a higher yield strength of 52 MPa, whereas, for FZ71, it is 47 MPa. Another remarkable point of the results is that the pure PLA sample presents a brittle behavior and breaks sharply after 2 mm displacement, but for the blends, the elongation at break increases. This phenomenon is attributed to the formation of immiscible phases, where PLA constitutes the continuous phase and PBS is the dispersed phase. The presence of the relatively flexible PBS serves to lower the brittleness of PLA. In practical terms, during tensile stress, the dispersed phases of soft PBS can act as stress concentrators, resulting in high-stress pockets in the PBS domains and leading to debonding in the blend. In summary, incorporating PBS into PLA/PBS blends proves beneficial for enhancing the elongation at break values of PLA, albeit at the expense of tensile yielding strength and stiffness.

The two grades of PBS in the blend show different elongation at break. For the blend with PBS FZ71, elongation continued up to 70% strain without the sample breaking; however, the test was halted due to equipment limitations. This higher elongation can be attributed to PBS FZ71's higher MFI, which allows for greater extension due to the presence of shorter polymer chains, improving flow and flexibility. In contrast, the blend containing PBS FZ91, with its lower MFI, only elongated to 8% strain.

Table 4. Thermal properties of 3D printed PLA and PLA/PBS samples.

Material	T_g	T_{cc}	T_m (PLA)	T_m (PBS)	ΔH_{cc}	ΔH_m (PBS)	ΔH_m (PLA)
Units	°C	°C	°C	°C	J g^{-1}	J g^{-1}	J g^{-1}
PLA	62.3	99.0	168.58	n/a	24.6	–	34.2
PLA/PBS FZ71	58.7	89.7	167.8	108.8	18.5	10.9	34.5
PLA/PBS FZ91	59.8	87.4	168.7	112.1	19.4	12.7	36.0

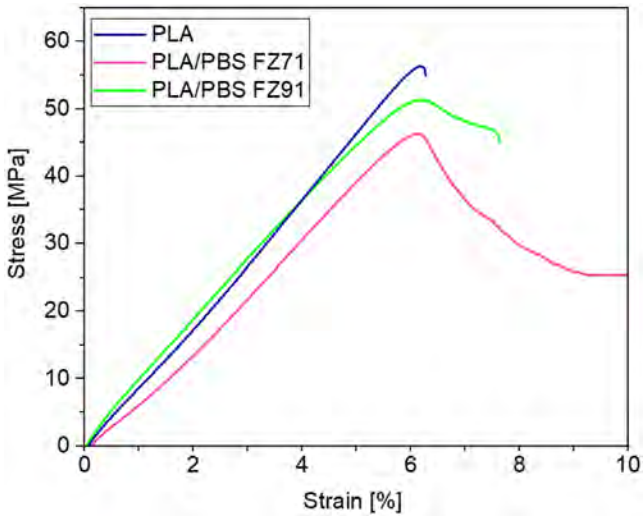

Figure 6. Stress–strain figures of tensile test on 3D printed samples.

3.5. Compression Tests

All samples are cyclically compressed to a specific displacement point, which corresponds to 50% of the sample's height, and then unloaded. During the unloading, they recovered some of their uncompressed initial shape (see Video 2, Supporting Information). The rest of the recovery process is done by dipping them in the water bath at 70 °C, which is above the glass transition temperature of the samples.

The area under the loading–unloading diagram represents the energy dissipation in the sandwich structures.[37,38] The amount of dissipated energy can be calculated from the force–displacement curve using the following equations

$$\text{Dissipate Energy} = \text{Stored Energy} - \text{Released Energy} = \int_0^{\delta_d} F d\delta - \int_{\delta_d}^{0} F d\delta \quad (2)$$

Based on the definition of dissipated energy, it can be derived from the difference between the stored and released energy. Equation (3) is employed to calculate the stored energy during loading, where δ_d represents the maximum length of the stroke during the quasistatic compression test and F denotes the compression force of displacement.

$$\text{Stored Energy} = \int_0^{\delta_d} F d\delta \quad (3)$$

Figure 7 presents an overview of the force–strain values alongside pictures of the sample at four different stages: the initial stage, maximum compression, after unloading, and at the end of the test, as well as a picture of the sample after recovery by thermal stimuli.

In **Figure 8**, the shape recovery ratio and dissipated energy rate for all 3D printed sandwich structures are displayed. Notably, PLA structures exhibit the highest compressive strength of 2647.85 N, while the PLA/PBS blends demonstrate lower mechanical strengths ranging between 2055.67 N for the blend with PBS FZ71 and 1779.89 N for the blend with PBS FZ91. A similar trend is observed for the dissipated energy rate, with PLA structures showing the highest value of 21 kJ. It is also evident that PLA/PBS samples exhibit lower dissipated energy values, ≈15 kJ for PBS FZ71 and 14 kJ for PBS FZ91, which are quite similar. PLA structures, as full-shape memory structures, boast the highest recovery ratio of 96%. However, with the addition of PBS, the shape recovery ratio decreases. The blend with PBS FZ91 shows a recovery of around 93%, while for the structures with PBS FZ71, this value is lower, at around 86% recovery. The

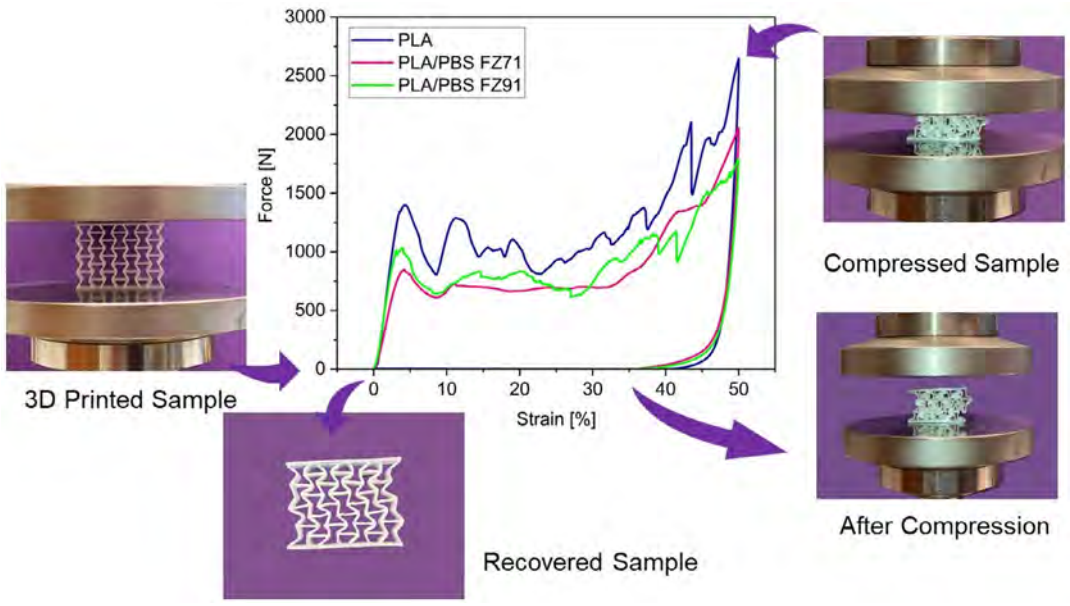

Figure 7. The force–strain data of cyclic compression of PLA and PLA/PBS fabricated samples, along with sample pictures at initial, maximum compression, after unloading, and after thermal recovery.

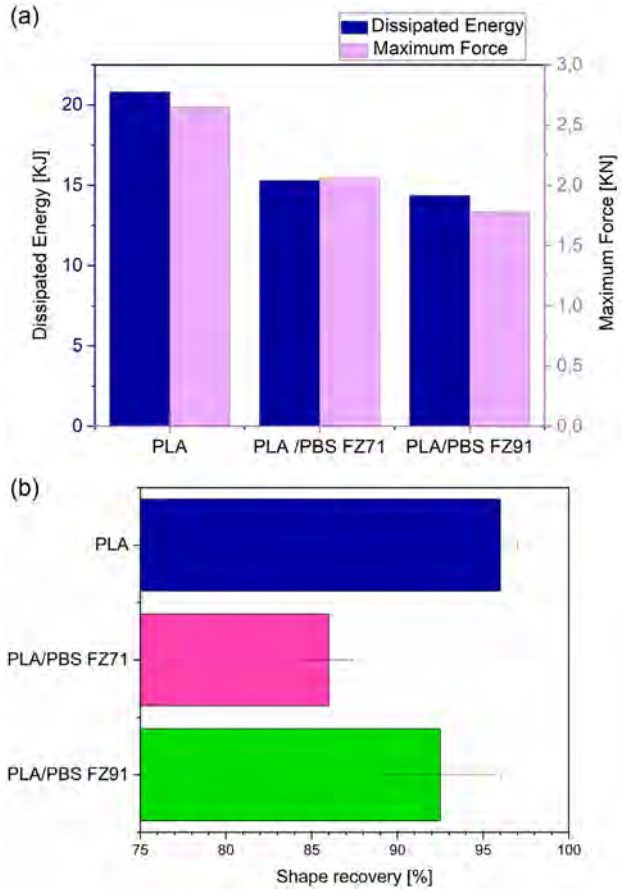

Figure 8. a) The results of the cyclic compressive test. Maximum compressive force and dissipated energy, and b) shape recovery ratio of all 3D printed sandwich structures, including PLA, PLA/PBS FZ71, and PLA/PBS FZ91.

significant difference in shape recovery ratio between these two blends, despite having the same amount of PBS and dissipating a similar amount of energy during cyclic compression, stems from the difference between their MFR and resulting MW. In the blend with PBS FZ71, the lower MW indicates that the polymer chains are shorter and less compact. Consequently, the compression process causes them to move more and change their initial state significantly. After activation by thermal stimuli, it becomes harder for the chains to return to their initial state, leading to a lower recovery compared to the blend with PBS FZ91.

The tensile tests showed that the addition of PBS FZ71 to PLA/PBS blend enhanced considerably not only elongation at break but also some thermal flow about one time higher than those from PLA, which is due mainly to its low MW and high melt index for characterizing weak intermolecular interactions in the amorphous region allowing chain mobility during processing. This is in full agreement with recent studies highlighting how variations of the polymer grade, especially MW and MFI, very markedly modify the mechanical properties of blends leading to higher flexibility.[39] Moreover, shape recovery tests of the PLLA/PBS blends with PBS FZ91 indicated an improvement in the ability to recover initial shape after deformation as opposed to the blend plasticized by lower viscosity filler, e.g., PBS FZ71. The difference is likely due to the larger MW of PBS FZ91 leading to improved stability and deformation resistance. This corroborates with previous reports that higher MW polymers generally demonstrate greater shape recovery, which is in part due to the improved chain entanglement and presence of larger polymeric chains.[40]

The compression tests showed that the PLA/PBS blend with PBS FZ71 had a slightly higher maximum compressive force and energy dissipation than the blend with PBS FZ91, likely due to its higher flexibility and lower chain length. These results are consistent with studies, showing that polymers with higher MFI and lower MW exhibit greater compressive strength and improved energy dissipation during mechanical stress.[41]

4. Conclusion

This study investigated the thermomechanical and functional properties of two PLA/PBS biopolymer blends with different PBS grades, namely, FZ71 and FZ91. Utilizing various manufacturing processes, the blends were initially melt-mixed, followed by extrusion, and subsequently 3D printed using the FFF technique to produce re-entrant sandwich structures. The microstructure, thermomechanical properties, and shape recovery of 3D printed samples are compared and studied. Here are several noteworthy discoveries identified in this investigation: 1) SEM images revealed that all the blends exhibit a sea–island structure, characterized by interactions between the dispersed PBS particles and the PLA matrix, indicating immiscibility within the blend. On the fracture surface, small holes can be observed where PBS particles were displaced during the fracturing process. The slight difference in the size of the dispersed phases between the two blends can be attributed to the viscosity ratio; as the viscosity ratio increases, the size of the dispersed phase also increases. The blend with PBS FZ71, which has a higher MFI, lower viscosity, and a higher viscosity ratio, corresponds to the observation of larger PBS domains within the matrix. 2) Thermal analysis revealed that the 3D printed PLA structure has a higher glass transition (T_g) and melting (T_m) temperatures compared to the PLA/PBS blends. The produced biopolymer blends also showed two melting temperatures corresponding to PLA and PBS in the blend. The peak temperature points and enthalpies were really close to each other, but the only difference between them was the heat flow exhibited during the test. The blend containing PBS FZ71 showed a vertical shift in heat flow toward the positive value which can be attributed to its higher MFI and shorter chain lengths, which facilitated the movement of the polymer chains. 3) Tensile tests demonstrated that blends containing PBS exhibited greater elongation at the break. In particular, the blend with PBS FZ71 elongated to 70% strain during the test and did not break. On the other hand, the blend containing the same amount of PBS but with a different grade, PBS FZ91, elongated less than 8% before the break due to the lower MFI and higher stiffness. 4) Compression tests highlighted that PLA possessed the highest maximum force, reflecting PLA ductility and stiff nature. For the blends, they demonstrated nearly identical behavior; for the blend with PBS FZ71, due to its higher

MFI and flexibility, the maximum compressive force was slightly higher than the one with PBS FZ91. The dissipated energy for PLA samples was the highest (21 kJ) and two blends dissipated near the same energy during the cyclic compression test (15 kJ) for the blend with PBS FZ71 and 14 kJ for the blend with PBS FZ91). The blend with PBS FZ71 grade showed higher dissipated energy as it is more flexible with lower chain length and more movements during compression. 5) Shape recovery varied between the two blends, even though they demonstrated identical maximum force and dissipated energy. The blend containing PBS FZ71, characterized by a lower MW, exhibited less ability to recover its initial state compared to the blend with PBS FZ91. This could be related to the chain lengths and their greater flexibility to change and move, making it harder for them to return to their initial state.

Supporting Information

Supporting Information is available from the Wiley Online Library or from the author.

Acknowledgements

The authors gratefully acknowledge the support received from the Applied Research SIA Foundation under the KIEM GoChem (GOCH.KIEM.KGC02.096) program. Special thanks are extended to Mr. Nick Helthuis and Mr. Bert Vos for their support in providing the microstructural and mechanical testing equipment for this study.

Conflict of Interest

The authors declare no conflict of interest.

Author Contributions

Ava Ghalayaniesfahani: Formal analysis (equal); Investigation (equal); Methodology (lead); Validation (lead); Writing—original draft (lead). **Betty Oostenbrink**: Formal analysis (equal); Investigation (equal); Visualization (equal). **Han van Kasteren**: Visualization (equal); Writing—review and editing (equal). **Mehrshad Mehrpouya**: Conceptualization (lead); Investigation (lead); Supervision (lead); Visualization (equal); Writing—review and editing (lead).

Data Availability Statement

The data that support the findings of this study are available from the corresponding author upon reasonable request.

Keywords

4D printing, biopolymer blends, energy absorption, polymer grades, shape memory polymers

Received: July 20, 2024
Revised: September 27, 2024
Published online:

[1] M. Mehrpouya, H. Vahabi, in *Additive Manufacturing of Biopolymers*, Elsevier, New York **2023**, pp. 1–10.
[2] A. C. L. de Morais, V. S. Voet, R. Folkersma, K. Loos, in *Additive Manufacturing of Biopolymers*, Elsevier, New York **2023**, pp. 39–63.
[3] A. Garmulewicz, F. Tourlomousis, C. Smith, P. Bolumburu, in *Additive Manufacturing of Biopolymers*, Elsevier, New York **2023**, pp. 371–399.
[4] C.-H. Chen, J.-S. Peng, M. Chen, H.-Y. Lu, C.-J. Tsai, C.-S. Yang, *Colloid Polym. Sci.* **2010**, *288*, 731.
[5] R. Muthuraj, M. Misra, A. K. Mohanty, *J. Polym. Environ.* **2014**, *22*, 336.
[6] A. V. Shenoy, D. R. Saini, *Adv. Polym. Technol.* **1986**, *6*, 1.
[7] Standard P 1133-1, *Plastics—Determination of the Melt Mass-Flow Rate (MFR) and the Melt Volume-Flow Rate (MVR) of Thermoplastics*, International Organization for Standardization, Geneva **2011**.
[8] M. J. John, N. Dyanti, T. Mokhena, V. Agbakoba, B. Sithole, *Materials* **2021**, *14*, 3462.
[9] M. Barletta, A. Gisario, M. Mehrpouya, *J. Manuf. Process.* **2021**, *61*, 473.
[10] L. Zeenat, A. Zolfagharian, M. Bodaghi, F. Pati, in *Additive Manufacturing of Biopolymers*, Elsevier, New York **2023**, pp. 191–227.
[11] M. Mehrpouya, W. M. Huang, in *Smart Materials in Additive Manufacturing, Volume 1: 4D Printing Principles and Fabrication*, Elsevier, New York **2022**, pp. 373–394.
[12] I. Gibson, D. W. Rosen, B. Stucker, M. Khorasani, D. Rosen, M. Khorasani, in *Additive Manufacturing Technologies*, Vol. *17*, Springer, Berlin **2021**.
[13] F. Carrasco, P. Pagès, J. Gámez-Pérez, O. O. Santana, M. L. Maspoch, *Polym. Degrad. Stab.* **2010**, *95*, 116.
[14] M. Mehrpouya, H. Vahabi, S. Janbaz, A. Darafsheh, T. R. Mazur, S. Ramakrishna, *Polymer* **2021**, *230*, 124080.
[15] B. Coppola, N. Cappetti, L. Di Maio, P. Scarfato, L. Incarnato, *Materials* **2018**, *11*, 1947.
[16] M. K. M. Haafiz, A. Hassan, Z. Zakaria, I. M. Inuwa, M. S. Islam, M. Jawaid, *Carbohydr. Polym.* **2013**, *98*, 139.
[17] N. Deoray, B. Kandasubramanian, *Polym. Plast. Technol. Eng.* **2018**, *57*, 860.
[18] M. Bartkowiak-Jowsa, R. Bedzinski, J. Chlopek, J. Filipiak, B. Szaraniec, *Polimery* **2011**, *56*, 224.
[19] Y. Phuphuak, Y. Miao, P. Zinck, S. Chirachanchai, *Polymer* **2013**, *54*, 7058.
[20] R. Somsunan, S. Noppakoon, W. Punyodom, *J. Polym. Res.* **2019**, *26*, 1.
[21] T. Yarici, M. Kodal, G. Ozkoc, *Polymer* **2018**, *146*, 361.
[22] M. Z. Ahmad Thirmizir, Z. A. Mohd Ishak, R. Mat Taib, K. S. K. C. Kanapathi Pillai, M. S. Salim, A. Hassan, M. B. Abu Bakar, *J. Vinyl Addit. Technol.* **2021**, *27*, 567.
[23] M. Barletta, C. Aversa, M. Ayyoob, A. Gisario, K. Hamad, M. Mehrpouya, H. Vahabi, *Prog. Polym. Sci.* **2022**, *132*, 101579.
[24] A. Ghalayaniesfahani, B. Oostenbrink, H. Van Kasteren, I. Gibson, M. Mehrpouya, *Polymer* **2024**, *307*, 127252.
[25] M. Barletta, M. Puopolo, *J. Manuf. Process.* **2020**, *56*, 1185.
[26] N. Nomadolo, O. E. Dada, A. Swanepoel, T. Mokhena, S. Muniyasamy, *Polymers* **2022**, *14*, 1894.
[27] A. Bhatia, R. K. Gupta, S. N. Bhattacharya, H. J. Choi, *Korea-Austr. Rheol. J.* **2007**, *19*, 125.
[28] S. Chuayjuljit, C. Wongwaiwattanakul, P. Chaiwutthinan, P. Prasassarakich, *Polym. Compos.* **2017**, *38*, 2841.
[29] W. Jiang, J. Zhou, J. Liu, M. Zhang, W. Huang, *Appl. Math. Modell.* **2023**, *116*, 547.
[30] M. Mehrpouya, T. Edelijn, M. Ibrahim, A. Mohebshahedin, A. Gisario, M. Barletta, *Adv. Eng. Mater.* **2022**, *24*, 2200677.
[31] Özen, K. Çava, H. Gedikli, Ü. Alver, M. Aslan, *Thin-Walled Struct.* **2020**, *156*, 106989.
[32] W. Zeng, W. Jiang, J. Liu, W. Huang, *Compos. Struct.* **2022**, *299*, 116084.
[33] X. Lu, J. Zhao, X. Yang, P. Xiao, *Polym. Test.* **2017**, *60*, 58.

[34] M. S. Thompson, S. Agarwal, R. K. Gupta, *J. Vinyl Addit. Technol.* **2022**, *28*, 104.
[35] S. C. Jana, M. Sau, *Polymer* **2004**, *45*, 1665.
[36] V. Everaert, L. Aerts, G. Groeninckx, *Polymer* **1999**, *40*, 6627.
[37] C. Wu, V. Nguyen-Van, P. Tran, *Mater. Sci. Addit. Manuf.* **2023**, *2*, 53.
[38] A. Serjouei, A. Yousefi, A. Jenaki, M. Bodaghi, M. Mehrpouya, *Smart Mater. Struct.* **2022**, *31*, 055014.
[39] W. Yu, L. Sun, M. Li, M. Li, W. Lei, C. Wei, *Polymers* **2023**, *15*, 4305.
[40] R. B. Da Cunha, S. N. Cavalcanti, P. Agrawal, G. De Figueiredo Brito, T. J. A. De Mélo, *J. Appl. Polym. Sci.* **2023**, *140*, 54561.
[41] M. H. Jandaghian, A. Sepahi, S. Hosseini, R. Esmaeilzade, E. Nikzinat, M. Masoori, K. Afzali, *J. Appl. Polym. Sci.* **2024**, *141*, e55078.